# Noise-induced desynchronization and stochastic escape from equilibrium in complex networks

M. Tyloo,[1,4] R. Delabays,[2,4] and Ph. Jacquod[3,4]

[1]*Institute of Physics, École Polytechnique Fédérale de Lausanne (EPFL), CH-1015 Lausanne, Switzerland*
[2]*Automatic Control Laboratory, Swiss Federal Institute of Technology, CH-8092 Zürich, Switzerland*
[3]*Department of Quantum Matter Physics, University of Geneva, CH-1211 Geneva, Switzerland*
[4]*School of Engineering, University of Applied Sciences of Western Switzerland HES-SO, CH-1951 Sion, Switzerland*

Complex physical systems are unavoidably subjected to external environments not accounted for in the set of differential equations that models them. The resulting perturbations are standardly represented by noise terms. If these terms are large enough, they can push the system from an initial stable equilibrium point, over a nearby saddle point, outside of the basin of attraction of the stable point. Except in some specific cases, the distance between these two points is not known analytically. Focusing on Kuramoto-like models and under simple assumptions on this distance, we derive conditions under which such noise terms perturb the dynamics strongly enough that they lead to stochastic escape from the initial basin of attraction. We numerically confirm the validity of that criterion for coupled oscillators on four very different complex networks. We find in particular that, quite counterintuitively, systems with inertia leave their initial basin faster than or at the same time as systems without inertia, except for strong white-noise perturbations.

## I. INTRODUCTION

Complex physical systems are mathematically modeled as dynamical systems. Equilibrium and steady states, if they exist, are determined and characterized by fixed points and limit cycles or tori of the corresponding differential equations [1]. For deterministic dynamical systems, the latter equations should be complemented by stochastic terms to account for unavoidable perturbations from unaccountable environmental degrees of freedom [2]. A central question of broad interest is to determine the magnitude and statistical properties of the relevant stochastic terms that could lead to the loss of equilibrium or induce transitions between different local equilibria. Some physically important situations where such stochastic escape phenomena may occur are electric power grids with high penetration of fluctuating renewable energy sources [3–5], superconducting rings [6], and Josephson junction arrays [7] subjected to noisy magnetic fields, as well as neuronal systems subjected to synaptic, ion-channel, neurotransmitter, or membrane potential noise [8,9].

Despite decades of investigations, theoretical studies of problems related to stochastic escape are generally extensions of the pioneering work of Kramers [10], which relates chemical reaction rates to action integrals between different potential minima. The problem is analytically tractable in low dimensions only (see also Ref. [11]), and several recent works considered noise-induced large fluctuations in the dynamical behavior of higher-dimensional network-coupled systems through the numerical determination of action-minimizing paths [5,12–14]. A better analytical understanding of the interplay of noise characteristics with the network topology is clearly desirable.

For some noisy coupled dynamical systems, escapes from a basin of attraction can be related to noise characteristics and to the topology of the interaction network. For sufficiently weak, bounded noise, fluctuations are small and there is no stochastic escape [15]. Noise makes the system fluctuate about its equilibrium, and typical deviation amplitudes can be evaluated from a linearized dynamics about the equilibrium [16–18]. The situation becomes fundamentally different for stronger noise. For Kuramoto-like models [Eq. (1)], with additive Ornstein-Uhlenbeck noise, this is illustrated in Fig. 1, which shows the time evolution of the winding number $q$ (defined in Sec. IV), characterizing different equilibrium fixed points. Changes in $q$ indicate that the system visits other basins of attraction, surrounding different equilibrium states. Below we use $q$ to detect transition from one basin to another. Depending on the oscillators' inertia and the noise amplitude and correlation time, this happens more or less quickly and for longer or shorter periods of time. Due to the high dimensionality of the state space and the nonlinear coupling between oscillators, the exact shape and size of the basins are impossible to capture [19–21]; consequently, the escape time
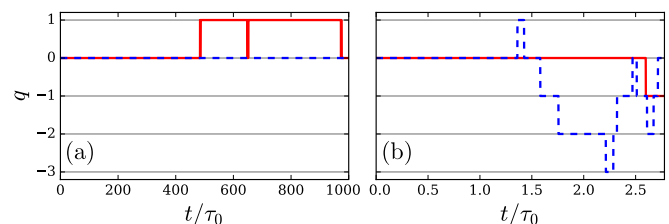


FIG. 1. Time evolution of the winding number $q$ for Eq. (1) on a single-cycle network with $n = 83$ nodes, $m = 0$ (red lines), and $\frac{m}{d} / \frac{d}{\lambda_2} = 10/175$ (blue dashed lines). (a) Noise with short correlation time $\lambda_2 \tau_0 / d = 5.7 \times 10^{-4}$. (b) Noise with longer correlation time $\lambda_2 \tau_0 / d = 0.03$.

from one basin is hard to predict. For the Kuramoto model with cyclic interactions, DeVille [12] showed that the escape time scales as the exponential of the potential barrier height between the initial and final equilibrium states. In the spirit of Kramers [10], Hindes and Schwartz [13,14] further relate the escape time to the numerically computed action on the action-minimizing trajectory between the two equilibria. In higher dimensions it is hard to see how these approaches could give analytical estimates other than in specific situations.

In this paper we propose a resolutely different approach to stochastic escape from stable equilibria in complex, network-coupled dynamical systems, incorporating noise characteristics as well as network dynamics and topology. We focus on synchronous fixed points of Kuramoto-like models [i.e., $\dot{\theta}_i(t) = \dot{\theta}_j(t), \forall i, j, t$] but stress that the approach is applicable to more general systems. We subject the initial, synchronous state to additive Ornstein-Uhlenbeck noise. Linearizing the dynamics about the synchronous state, we calculate the standard deviation of the noise-induced fluctuations about that state. The linearized dynamics is no longer accurate when the standard deviation exceeds some threshold distance $D_c$. Clearly $D_c$ is bounded from above by the distance $\Delta$ between the stable synchronous state and the closest saddle point to the next basin of attraction. We postulate that $D_c$ is parametrically proportional to $\Delta$. This postulate allows us to derive a criterion for stochastic escape based on the distance $\Delta$ between the initial stable synchronous fixed point and the nearest saddle point and not as in Kramers' and other approaches [5,10,12–14] on their potential height difference. We validate numerically our postulate that $D_c \sim \Delta$ for four, very different networks and furthermore show that it gives precise estimates for the first stochastic escape time. We note that similar linearization procedures have been used in a different context in Ref. [22] to predict transitions in an evolutionary ecology model.

The paper is organized as follows. In Sec. II we introduce our model of coupled oscillators and give analytical expressions for the response induced by noisy perturbations. Section III describes our criterion for stochastic escapes, and Sec. IV illustrates numerically our theory. Our conclusions are given in Sec. V.

## II. THE MODEL

We consider generic, Kuramoto-like models of nonlinearly coupled oscillators on complex graphs defined by the differential equations [23]

$$m\,\ddot{\theta}_i + d\,\dot{\theta}_i = P_i - \sum_j b_{ij} \sin(\theta_i - \theta_j). \quad (1)$$

Oscillators with inertia $m$ and damping parameter $d$ are described by compact angle coordinates $\theta_i \in (-\pi, \pi]$ and natural frequencies $P_i \in \mathbb{R}$. They are located on nodes $i = 1, \ldots, n$ of a connected coupling network defined by the adjacency matrix, $b_{ij} \geqslant 0$. Without loss of generality, we consider $\sum_i P_i = 0$, which is equivalent to considering the system in a rotating frame, because Eq. (1) is invariant under $\theta_i(t) \to \theta_i(t) + \Omega t, P_i \to P_i + d\,\Omega$. For bounded distributions of natural frequencies on small enough intervals, synchronous states exist with $\dot{\theta}_i \equiv 0, \forall i$.

We consider a stable synchronous state $\boldsymbol{\theta}^{(0)} = (\theta_1^{(0)}, \ldots, \theta_n^{(0)})$ corresponding to natural frequencies $\boldsymbol{P}^{(0)}$. We subject this state to a time-dependent perturbation $\boldsymbol{P}(t) = \boldsymbol{P}^{(0)} + \delta\boldsymbol{P}(t)$. Linearizing the dynamics defined by Eq. (1) with $\boldsymbol{\theta}(t) = \boldsymbol{\theta}^{(0)} + \delta\boldsymbol{\theta}(t)$, one obtains

$$m\,\ddot{\delta\boldsymbol{\theta}} + d\,\dot{\delta\boldsymbol{\theta}} \approx \delta\boldsymbol{P} - \mathbb{L}\big(\{\theta_i^{(0)}\}\big)\,\delta\boldsymbol{\theta}, \quad (2)$$

with the weighted Laplacian $\mathbb{L}(\{\theta_i^{(0)}\})$ defined by

$$\mathbb{L}_{ij} = \begin{cases} -b_{ij} \cos\big(\theta_i^{(0)} - \theta_j^{(0)}\big), & i \neq j, \\ \sum_k b_{ik} \cos\big(\theta_i^{(0)} - \theta_k^{(0)}\big), & i = j. \end{cases} \quad (3)$$

This matrix is positive semidefinite, with a single eigenvalue $\lambda_1 = 0$ and associated eigenvector $\mathbf{u}_1 = (1, 1, 1, \ldots, 1)/\sqrt{n}$, while $\lambda_\alpha > 0, \alpha = 2, 3, \ldots, n$.

The dynamics of Eq. (2) is characterized by different timescales. The first one characterizes the noisy perturbations. We consider spatially uncorrelated noise with vanishing average and Ornstein-Uhlenbeck correlator

$$\langle \delta P_i(t)\,\delta P_j(t') \rangle = \delta_{ij}\,\delta P_0^2\,\exp[-|t - t'|/\tau_0]. \quad (4)$$

Thus, the perturbation is characterized by its variance, $\delta P_0^2$ and its correlation time, $\tau_0 > 0$. The second timescale is $m/d$. It gives the typical time over which local excitations are damped by $d$, neglecting the network dynamics. Finally, one has a set of timescales $d/\lambda_\alpha, \alpha = 2, \ldots, n$, each of them defined by the ratio of the damping parameter and an eigenvalue of the Laplacian. For $m/d > d/4\lambda_\alpha$ these are related to oscillation timescales of the Laplacian modes, while for $m/d < d/4\lambda_\alpha$ they relate to network-dynamical corrections to the damping timescale. We consider $\tau_0$ as a tunable parameter allowing us to explore different regimes depending on its relation with $m/d$ and $d/\lambda_\alpha$.

We measure the distance between the state of the system and the initial synchronous state as the square root of the variance $\langle \delta\boldsymbol{\theta}^2(t) \rangle = \sum_i \langle [\delta\theta_i(t) - \overline{\delta\theta}(t)]^2 \rangle$ with $\overline{\delta\theta}(t) = n^{-1} \sum_i \delta\theta_i(t)$ and brackets indicating an average over different realizations of noise with the same first two moments. It appropriately gives the standard deviation of the angle deviations in the subspace orthogonal to $\mathbf{u}_1$, because displacements in that subspace do not change the state. To calculate $\langle \delta\boldsymbol{\theta}^2(t) \rangle$, we expand angle deviations over the eigenbasis of $\mathbb{L}$ and solve Eq. (2) for the coefficients of that expansion [24, Appendix A]. We obtain the long-time limit

$$\lim_{t \to \infty} \langle \delta\boldsymbol{\theta}^2(t) \rangle = \delta P_0^2 \sum_{\alpha \geqslant 2} \frac{\tau_0 + m/d}{\lambda_\alpha(\lambda_\alpha \tau_0 + d + m/\tau_0)}. \quad (5)$$

In the two limits of long and short $\tau_0$, one has

$$\lim_{t \to \infty} \langle \delta\boldsymbol{\theta}^2(t) \rangle \simeq \begin{cases} \frac{\delta P_0^2 \tau_0}{nd} Kf_1, & \tau_0 \ll \frac{d}{\lambda_\alpha}, \frac{m}{d}, \\ \frac{\delta P_0^2}{n} Kf_2, & \tau_0 \gg \frac{d}{\lambda_\alpha}, \frac{m}{d}, \end{cases} \quad (6)$$

with $Kf_p = n \sum_{\alpha \geqslant 2} \lambda_\alpha^{-p}$ [17,25]. Interestingly, none of these asymptotics depend on inertia.
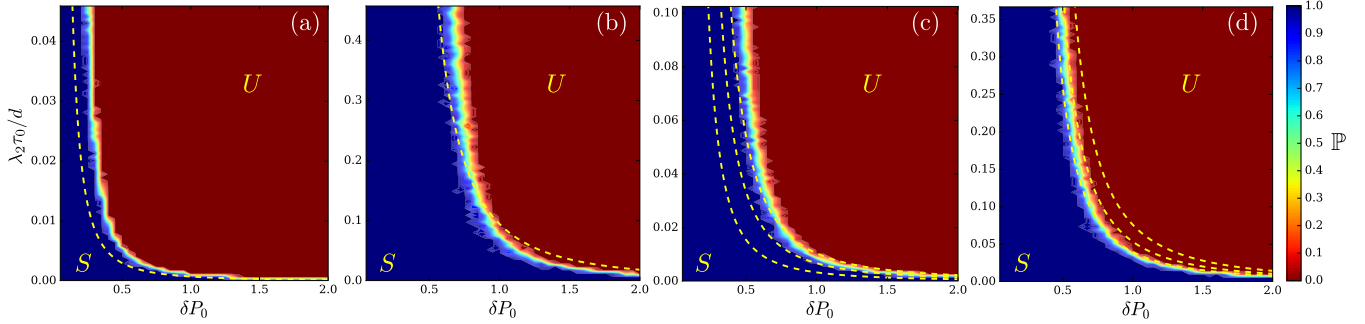
FIG. 2. Color-coded survival probability $\mathbb{P}$ for Eq. (1) with $m = 0$. (a) Single-cycle network with $n = 83$ and nearest-neighbor coupling; (b) single-cycle network with $n = 83$, nearest- and third-neighbor coupling; (c) U.K. transmission network with $n = 120$; (d) small-world network with $n = 200$ nodes. Yellow dashed lines give the boundary of the region of validity of the inequality in Eq. (8) with $m = 0$ and $\Delta$ obtained analytically for panel (a) and numerically for panels (b)–(d). Observation times $T_{\text{obs}}$ correspond to comparable dimensionless parameters $\lambda_2 T_{\text{obs}}/d = 143$ (a), 143 (b), 130 (c), and 115 (d).

## III. ESCAPE FROM THE BASIN

The dynamics of Eq. (1) is described by a vector function $\boldsymbol{\theta}(t)$ following the gradient of the potential

$$\mathcal{V}(\boldsymbol{\theta}, t) = \sum_{i=1}^{n} P_i(t)\theta_i - \sum_{i,j} b_{ij}[1 - \cos(\theta_i - \theta_j)], \quad (7)$$

starting from $\boldsymbol{\theta}(t = 0) = \boldsymbol{\theta}^{(0)}$. When the noisy perturbation tilts this potential strongly enough, $\boldsymbol{\theta}$ can escape the basin of attraction of $\boldsymbol{\theta}^{(0)}$. DeVille showed that, for not too large $\delta P_0$, the system almost surely escapes the basin in a neighborhood of a saddle point with a unique unstable direction, which we call 1-saddle [12]. Comparing the typical distance between $\boldsymbol{\theta}$ and $\boldsymbol{\theta}^{(0)}$ of Eq. (5) with the distance $\Delta$ between $\boldsymbol{\theta}^{(0)}$ and its closest 1-saddle $\boldsymbol{\varphi}$ gives us a parametric condition for noise-induced stochastic escape

$$\delta P_0^2 \sum_{\alpha \geqslant 2} \frac{\tau_0 + m/d}{\lambda_\alpha(\lambda_\alpha \tau_0 + d + m/\tau_0)} \leqslant \Delta^2. \quad (8)$$

Our task is therefore to identify the position of the 1-saddles. This is in general no trivial task because the geometry of basins of attraction in such high-dimensional problems is impossible to fully capture. For single-cycle networks with identical frequencies, 1-saddles can be identified analytically [12,21]. For more general networks, we give in Appendix D a numerical algorithm which locates 1-saddles $\boldsymbol{\varphi}$ and constructs the distribution of their distance to $\boldsymbol{\theta}^{(0)}$.

## IV. NUMERICAL SIMULATIONS

We first check Eq. (8) against numerical simulations of the Kuramoto model of Eq. (1) with $m = 0$. We consider four different networks (see Appendix C) with constant couplings $b_0 = 1$ and identical frequencies, which are a single-cycle network with nearest-neighbor coupling, a single-cycle with nearest- and third-neighbor coupling, a model of the U.K. transmission network, and a realization of a small-world network [26]. At each node, natural frequencies are perturbed by spatially uncorrelated Gaussian noisy sequences $\delta P_i(t)$ satisfying Eq. (4). We integrate the dynamics of Eq. (1), using a fourth-order Runge-Kutta method, during an observation

time $T_{\text{obs}}$ and check for a stochastic escape at every time step. Our method for detecting such occurrences is based on Refs. [27–29], which showed that on meshed networks, different fixed-point solutions of Eq. (1) correspond to different vectors of winding numbers $\boldsymbol{q}$. While winding around a cycle of a meshed network, the sum of angle differences is an integer multiple of $2\pi$. This integer is the winding number $q$ on the corresponding cycle of the interaction graph. Such winding numbers can be defined on each cycle of the network and form together a winding vector $\boldsymbol{q}$.

References [12,14] observed that transitions between different such equilibrium states occur by phase slips of few oscillators, and we show in Appendix B that these slips can be detected by recording the time evolution of $\boldsymbol{q}$, as illustrated in Fig. 1. We therefore detect desynchronizing events through variations of winding numbers. For each set of noise parameters $\delta P_0$ and $\tau_0$ we perform several calculations corresponding to different noise realizations.

Figure 2 shows the fraction $\mathbb{P}$ of runs that remain in the initial basin for $t \leqslant T_{\text{obs}}$. The parameter space is sharply divided into (a) the red region (denoted $U$ for "unstable") where all runs left the basin of attraction before $T_{\text{obs}}$, (b) the blue region (denoted $S$ for "stable"), where none of the runs left the initial basin of attraction, and (c) a rather narrow intermediate region between $U$ and $S$ where some runs left and some runs stayed in the initial basin.

It is quite remarkable that the intermediate region (c) is qualitatively if not quantitatively identified by Eq. (8) with a network-dependent $\Delta$. As discussed above, $\Delta$ is given by a typical distance between the initial stable fixed point $\boldsymbol{\theta}^{(0)}$ and the nearest saddle point $\boldsymbol{\varphi}$ roughly giving the smallest linear size of the basin of attraction. For the single-cycle network, all 1-saddles are located at the same distance from $\boldsymbol{\theta}^{(0)}$, which can be obtained analytically [12]. For the other three networks, many, though likely not all, 1-saddles are identified numerically. The detailed methods for finding 1-saddles are given in Appendix D. For the single-cycle network with nearest- and third-neighbor coupling, the distance $\Delta$ from $\boldsymbol{\theta}^{(0)}$ takes only a few different values of which we consider only the most representative. For the U.K. and small-world networks, on the other hand, we find a distribution of $\Delta \in [\Delta_{\min}, \Delta_{\max}]$, which is likely due to the complexity of those meshed networks.
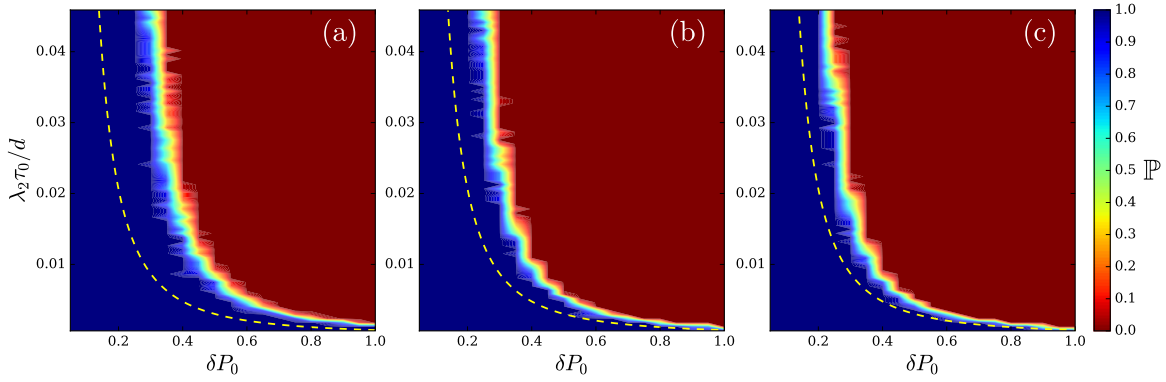
FIG. 3. Color-coded survival probability $\mathbb{P}$ for Eq. (1) with $m = 0$ for a single-cycle network with $n = 83$ and nearest-neighbor coupling; $\lambda_2 T_{\text{obs}}/d = 14.3$ (a), 143 (b), 569 (c). The yellow dashed line gives the boundary of the region of validity of the inequality in Eq. (8) with $m = 0$ and $\Delta$ obtained analytically.

The yellow dashed lines in Fig. 2 then indicate our theoretical prediction Eq. (8) for the obtained value $\Delta$ for the two single-cycle networks and for values of $\Delta$ corresponding to the 25th, 50th, and 75th percentiles of the distribution of $\Delta$ for the U.K. and small-world networks. In all cases, the shape of the boundary is well predicted. For the more complex U.K. transmission network [Fig. 2(c)], there is a horizontal shift between theory and numerics, presumably due to to stronger anisotropies of the basins of attraction in this more complex network, effectively requiring a larger $T_{\text{obs}}$.

In the case of bounded noise, we expect an inertialess system to remain in its initial basin for weak enough noise [15]. However, the noise considered in our case is Gaussian, and arbitrarily large excursion will occur if one waits long enough. In fact, we found that increasing $T_{\text{obs}}$ shifts the boundary between stable and unstable regions to lower $\delta P_0$. We evaluated the influence of the observation time by reproducing Fig. 2(a) with different $T_{\text{obs}}$. This is shown in Fig. 3 where we performed simulations for the cycle, increasing the observation time. Figure 3 shows the fraction of simulations that stay in the initial basin of attraction after an observation time satisfying $\lambda_2 T_{\text{obs}}/d = 14.2$ [Fig. 3(a)], 142.4 [Fig. 3(b)], 569 [Fig. 3(c)], for a cycle network with $n = 83$ nodes. As $T_{\text{obs}}$ increases exponentially, we observe the boundary between regions $U$ and $S$ drifting to the left due to the escape time that is superexponential as $\delta P_0$ decreases.

Figure 4 further shows the stochastic escape time as a function of $\delta P_0$. A superexponential behavior is observed

which can be understood as follows. The noise generates a distribution of angle deviations which we expect to be Gaussian with a variance given by Eq. (5). The escape time is then inversely proportional to the probability to have such a deviation exceeding $\Delta$,

$$T_{\text{esc}} \propto \left[ 2 \int_{\beta\Delta}^{\infty} P\left(\overline{\delta\theta}\right) d\left(\overline{\delta\theta}\right) \right]^{-1}, \qquad (9)$$

with a free parameter $\beta$ of order 1. Figure 4 validates this argument using a Gaussian distribution of single-angle deviation $P(\overline{\delta\theta})$ with variance $\langle \delta\theta^2(t) \rangle / n$; see Eq. (5). We have found, but do not show, that $T_{\text{esc}}$ diverges at a finite value of $\delta P_0$ for a box-distributed, bounded noise.

We finally consider Eq. (1) with nonzero inertia. We focus on the single-cycle network with nearest- and third-neighbor coupling and tune the inertia parameter $m$ to explore different regimes defined by the different timescales of Eq. (1). Figure 5 shows the difference in survival probabilities with and without inertia in the regimes (a) $d/\lambda_\alpha \gtrsim m/d$, (b) $d/\lambda_\alpha \lesssim m/d$, and (c) $d/\lambda_\alpha \ll m/d$. Deep in the stable (unstable) regions, both inertialess and inertiaful models have $\mathbb{P} = 0$ ($\mathbb{P} = 1$) and the difference $\mathbb{P}(m = 0) - \mathbb{P}(m) = 0$. Somehow counterintuitively, however, there is an intermediate region where the presence of inertia facilitates stochastic escape compared to the inertialess case, $\mathbb{P}(m = 0) - \mathbb{P}(m) > 0$. The boundary of that region are in excellent agreement with the prediction of Eq. (8), giving the two dashed yellow lines for $m = 0$ and $m \neq 0$.
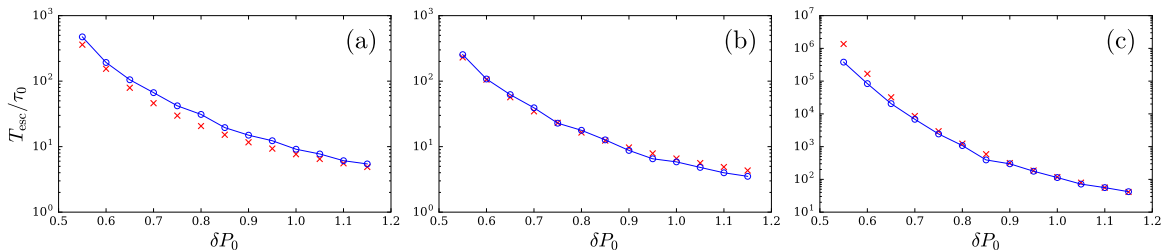


FIG. 4. Escape time $T_{\text{esc}}$ from the initial basin of attraction vs noise amplitude, $\delta P_0$, for cycle networks with $n = 83$ (a), $n = 249$ (b), and the U.K. transmission network (c). The noise correlation time corresponds to $\lambda_2 \tau_0/d = 8.6 \times 10^{-3}$ (a), $\lambda_2 \tau_0/d = 9.6 \times 10^{-4}$ (b), and $\lambda_2 \tau_0/d = 0.02$ (c). Blue circles are averages over 40 realizations of noise. Red crosses correspond to Eq. (9), with $\beta \cong 5/8$ (a, b) and $\beta \cong 2/5$ (c).
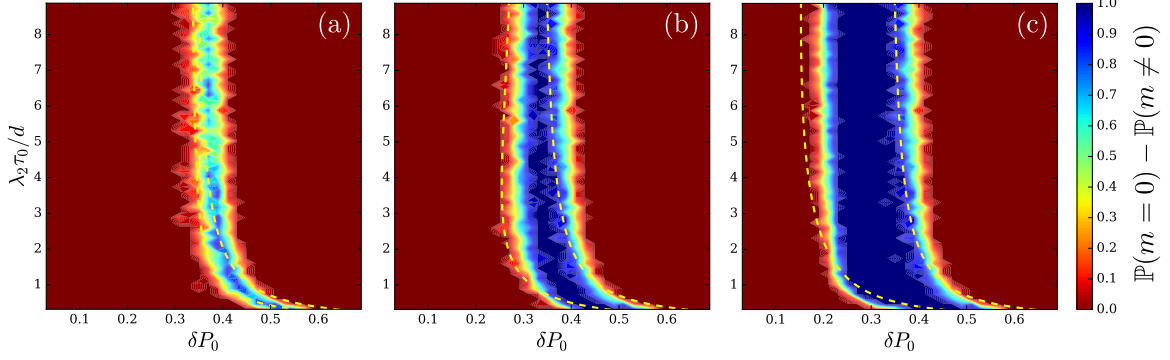
FIG. 5. Color-coded difference in survival probability $\mathbb{P}$ with and without inertia for a single-cycle network with $n = 83$ with nearest- and third-neighbor coupling obtained from 20 realizations of noise; (a) $\frac{m}{d}/\frac{d}{\lambda_2} = 0.25/0.35$, (b) 2.5/0.35, and (c) 25/0.35. The yellow dashed lines give the boundary of the region of validity of the inequality in Eq. (8), as discussed in the main text.

For large $\tau_0$, the faster escape of the system with finite inertia is easily understood. With long correlation time, the noise tends to push the system in the same direction for long sequences. This is sufficient to have the inertiaful system accumulate a significant kinetic energy. The system keeps then moving, even if, after some time, the noise starts pushing the other way and allows it to move above a saddle point with inertia, whereas the inertialess system is immediately stopped by noise reversal.

For smaller $\tau_0$, on the other hand, inertia resists short sequences of pushes in rapidly varying directions and accordingly, we found that inertia stabilizes the system in that case (see Appendix E). This is not predicted by Eq. (8) and is probably due to contributions beyond our linear response theory, because discrepancies appear for values of $\delta P_0$ comparable to the coupling strength $b_0$. The influence of inertia on stochastic escapes is perhaps best illustrated in Fig. 1, where the presence of inertia stabilizes the system under short-correlated noise [Fig. 1(a)] but leads to more frequent stochastic escapes for long-correlated noise [Fig. 1(b)].

## V. CONCLUSION

We have constructed an alternative to stochastic escape. We compare a spectral calculation of typical sizes of stochastic excursions about synchronous equilibrium states with an evaluation of the distance between this synchronous equilibrium state and 1-saddles. This method provides analytical results with a single, model-dependent free parameter of order one [$\beta$ in Eq. (9)]. It gives remarkably accurate estimates for stochastic escape times, as is illustrated in Fig. 4. Even if, in this work, we considered networks of coupled oscillators, our method can be applied to any dynamical system where some stable fixed points and 1-saddles are available, and the linearization of the dynamics in a neighborhood of the considered fixed point is possible. The distance $\Delta$ between stable fixed points and 1-saddles and the eigenvalues of the linearization of the dynamical system are the main ingredients of Eq. (8), which determine regions where escape is unlikely in reasonable time.

In the context of coupled oscillators, we interestingly observed that the presence of inertia leads to faster, more frequent escapes for long noise coherence times, while the

effect is reversed for short noise coherence times. This is illustrated in Fig. 1. Further studies should consider the effect of spatially correlated noise and non-Gaussian, long-tailed noise distributions [18].

## APPENDIX A: DETAILS OF CALCULATIONS FOR THE VARIANCE OF THE ANGLE DISPLACEMENTS

We give some details of the calculation that leads to Eq. (5). Expanding the angle deviations over the eigenmodes of the Laplacian Eq. (3), $\delta\boldsymbol{\theta}(t) = \sum_\alpha c_\alpha(t)\mathbf{u}_\alpha$, Eq. (2) becomes

$$m\,\ddot{c}_\alpha(t) + d\,\dot{c}_\alpha(t) = \delta\boldsymbol{P}(t) \cdot \mathbf{u}_\alpha - \lambda_\alpha c_\alpha(t), \quad \alpha = 2, \ldots, n.$$
(A1)

With the help of a Laplace transform, the solution of Eq. (A1) is given by

$$c_\alpha(t) = m^{-1} e^{\frac{-d/m - \Gamma_\alpha}{2}t} \int_0^t e^{\Gamma_\alpha t'}$$
(A2)

$$\times \int_0^{t'} \delta\boldsymbol{P}(t'') \cdot \mathbf{u}_\alpha e^{\frac{d/m - \Gamma_\alpha}{2}t''} dt''dt',$$
(A3)

with $\Gamma_\alpha = \sqrt{(d/m)^2 - 4\lambda_\alpha/m}$. Taking advantage of the orthogonality between eigenmodes of the Laplacian we have

$$\langle\delta\boldsymbol{\theta}^2(t)\rangle \equiv \sum_i \langle[\delta\theta_i(t) - \delta\bar{\theta}(t)]^2\rangle = \sum_{\alpha\geqslant 2}\langle c_\alpha^2(t)\rangle,$$
(A4)

with $\delta\bar{\theta}(t) = n^{-1}\sum_i \delta\theta_i(t)$. Inserting Eq. (A1) into Eq. (A4), using the time correlator of $\delta\boldsymbol{P}$ Eq. (4), and finally taking the long-time limit, one obtains, after some algebra, Eq. (5).

## APPENDIX B: METHOD TO DETERMINE ESCAPE TIME

Various methods can be used to determine, at any iteration step of the simulation, if the system under consideration has escaped its initial basin of attraction. We compared three of them, which we detail here.

TABLE I. Final winding number $q^{(1)}$ and number of iterations before the escape for $m = 0$ (simulations 1–3) and finite inertia (simulations 4–6). Each triplet is obtained by integrating Eq. (1) with the same noise sequence.

| Simulation | 1 | | | 2 | | | 3 | | | 4 | | | 5 | | | 6 | | |
|---|---|---|---|---|---|---|---|---|---|---|---|---|---|---|---|---|---|---|
| Method | 1 | 2 | 3 | 1 | 2 | 3 | 1 | 2 | 3 | 1 | 2 | 3 | 1 | 2 | 3 | 1 | 2 | 3 |
| $q^{(1)}$ | −1 | −1 | −1 | −1 | −1 | −1 | −1 | −1 | −1 | 1 | 1 | −1 | −1 | −1 | −1 | 1 | 1 | −1 |
| No. of iterations | 400 | 400 | 400 | 685 | 685 | 685 | 558 | 558 | 550 | 1609 | 1609 | 950 | 1664 | 1664 | 1249 | 1887 | 1887 | 1151 |

*Method 1.* As stated in the main text, stable equilibria of Eq. (D1) below can be unambiguously distinguished by their winding vector $\boldsymbol{q}$. The method that we used for the numerical simulations in the main text proceeds as:

(1) At each time step, compute $\boldsymbol{q}$.

(2) If $\boldsymbol{q} \neq \boldsymbol{q}^{(0)}$ the winding vector of the initial basin of attraction, check if the system is still in the initial basin. To do so, simulate the dynamics without noise, taking the current state of the system as initial conditions. Once synchrony is reached, compute the winding vector $\boldsymbol{q}^{(1)}$.

(3) If $\boldsymbol{q}^{(1)} \neq \boldsymbol{q}^{(0)}$, then the system was out of the initial basin. Otherwise, if $\boldsymbol{q}^{(1)} = \boldsymbol{q}^{(0)}$, the system was still in the basin, and thus the simulation can move to the next time step.

*Method 2.* This method is based on DeVille's observation [12] that escapes from basins of attraction occur on a short time interval and can be identified by a fast slip of a small group of angles. It proceeds as

(1) At each time step, check if some angles made a large excursion, i.e., $\|\boldsymbol{\theta}(t) - \boldsymbol{\theta}^{(0)}\|_\infty > 2\pi$.

(2) If so, then simulate the dynamics without noise, taking the current state of the system as initial conditions, until it synchronizes to the state $\boldsymbol{\theta}^{(1)}$.

(3) If $\boldsymbol{\theta}^{(1)} \neq \boldsymbol{\theta}^{(0)}$, then the system was out of the initial basin. Otherwise, if $\boldsymbol{\theta}^{(1)} = \boldsymbol{\theta}^{(0)}$, the system was still in the basin, and thus the simulation can move to the next time step.

*Method 3.* Finally, we tested the method in which we check at every time step whether the system returns to the initial basin or not. This method guarantees to find the best estimate of the escape time, at least for the Kuramoto model ($m = 0$), but is very time-consuming.

Table I compares escape times and final winding numbers for a single cycle of $n = 83$ nodes. For the Kuramoto model ($m = 0$) the three methods give very similar results. For the case with inertia, the first two give larger escape times compared to the last method. We explain this as follows. When the noise is removed, the system may have accumulated some kinetic energy that will drive it out of the basin of attraction. This can happen before the winding number changes or a large angle excursion occurs. Furthermore, if the perturbation was still active, it could have pushed the system back towards the stable fixed point before it leaves the basin of attraction, increasing the escape time.

## APPENDIX C: THE FOUR NETWORKS

We briefly describe the networks used for the numerical simulations of the main text.

### 1. Cycle with nearest neighbors coupling

We consider a cycle network of size $n$, with identical natural frequencies. The eigenvalues of its weighted Laplacian [Eq. (3)] can be obtained analytically,

$$\lambda_\alpha = \cos(\delta)[2 - 2\cos(k_\alpha)], \quad \alpha = 1, \ldots, n, \quad (C1)$$

where $\delta$ is the angle difference between neighboring sites (which are identical at a stable equilibrium [30]) and $k_\alpha = 2\pi(\alpha - 1)n^{-1}$. For $n = 83$ we have $\lambda_\alpha \in [0, 4\cos(\delta)]$ and $\lambda_2 = 0.0057$.

Equation (6) can be explicitly calculated for cyclic networks as functions of the number of nodes $n$:

$$\delta P_0^2 \leqslant \frac{\pi^2 dn}{\tau_0(n-2)^2}, \quad \tau_0 \ll d/\lambda_\alpha, m/d, \quad (C2)$$

$$\delta P_0^2 \leqslant \frac{60\pi^2 n}{(n-2)^2(n^2+11)}, \quad \tau_0 \gg d/\lambda_\alpha, m/d. \quad (C3)$$

Figure 6 shows the maximum values of $\delta P_0$ satisfying Eqs. (C2) and (C3). One remarks that, while increasing the size of the cycle, the stable region gets smaller and even vanishes for $n \to \infty$ similarly to fluctuations that destroy long-range order in one-dimensional locally interacting quantum magnets [31].
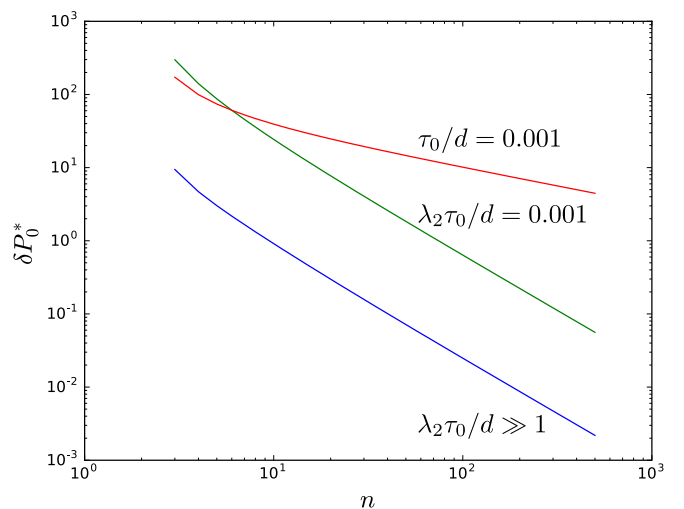


FIG. 6. Maximum value $\delta P_0^*$ of the noise amplitude obtained from Eqs. (C2) and (C3) for large (blue) and short (green, red) time correlation, $\tau_0$, as a function of the size of the cyclic network $n$. For the red curve, we consider a constant ratio $\tau_0/d = 0.001$. For the green curve we consider a constant ratio $\lambda_2\tau_0/d = 0.001$ where $\lambda_2 = 2 - 2\cos(2\pi/n)$ depends on the size of the network.
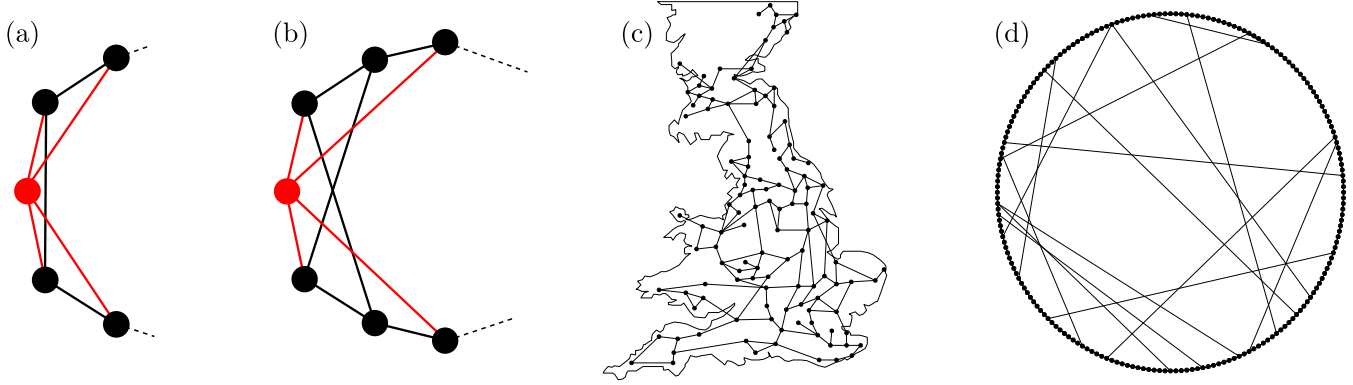
FIG. 7. (a) Illustration of the connections of a vertex to its first and second neighbors on a cycle. (b) Illustration of the connections of a vertex to its nearest and third neighbors on a cycle. (c) Illustration of the U.K. network with $n = 120$ vertices and $m = 165$ edges. (d) Illustration of our small-world network with $n = 200$ vertices. Its relative clustering coefficient is $C(\mathcal{G}_p)/C(\mathcal{G}_0) \approx 0.89$, and its relative characteristic path length is $L(\mathcal{G}_p)/L(\mathcal{G}_0) \approx 0.32$.

### 2. Cycle with nearest- and third-neighbor coupling

We consider a cycle network of size $n$, where each vertex is connected to its nearest and third neighbors [see Fig. 7(b)]. With identical natural frequencies, the eigenvalues of its weighted Laplacian [Eq. (3)] can be obtained analytically,

$$\lambda_\alpha = \cos(\delta)[4 - 2\cos(k_\alpha) - 2\cos(3k_\alpha)], \quad \alpha = 1, \ldots, n, \tag{C4}$$

where $\delta$ is the angle difference between neighboring sites (which are identical at a stable steady state [30]) and $k_\alpha = 2\pi(\alpha - 1)n^{-1}$. For $n = 83$ we have $\lambda_\alpha \in [0, 8\cos(\delta)]$ and $\lambda_2 = 0.057$.

### 3. U.K. transmission grid

A model of the U.K. electrical transmission grid is depicted in Fig. 7(c). It is composed of 120 nodes and 165 edges, making 44 cycles. During the numerical simulations, to check whether the system has left the initial basin of attraction or not, we check the winding number on each cycle, i.e., the winding vector $\boldsymbol{q} = (q_1, \ldots, q_{44})$. The second eigenvalue of its Laplacian matrix is $\lambda_2 \approx 0.013$.

### 4. Small-world

A small-world network is constructed from an initial network, where some edges are randomly rewired (see Ref. [26]). In our case, the initial network $\mathcal{G}_0$ is a cycle with $n = 200$
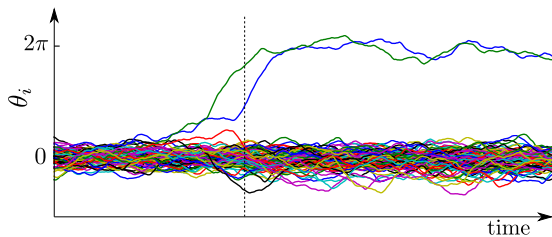


FIG. 8. Example of the time evolution of the 120 angles of the U.K. network [Fig. 7(c)]. We clearly see two angles jumping from a value close to 0 to a value close to $2\pi$. The state of the system at the time given by the vertical dashed line is our candidate for a 1-saddle $\boldsymbol{\varphi}$.

vertices and where each vertex is connected to its first and second neighbors [see Fig. 7(a)]. Each edge $(i, j)$ is then replaced with probability $p = 0.05$ by the edge $(i, k)$, where $k$ is chosen at random among the vertices not already connected to $i$. The network obtained $\mathcal{G}_p$ is illustrated in Fig. 7(d). It is a small world because it has a large relative clustering coefficient $C(\mathcal{G}_p)/C(\mathcal{G}_0) \approx 0.89$ and a small relative characteristic path length $L(\mathcal{G}_p)/L(\mathcal{G}_0) \approx 0.32$ (see Ref. [26] for more details). The second eigenvalue of its Laplacian matrix is $\lambda_2 \approx 0.046$.

### APPENDIX D: FINDING 1-SADDLES

We detail our methods for finding 1-saddles (equilibria with a unique unstable direction) of the dynamical system

$$m_i\ddot{\theta}_i + d_i\dot{\theta}_i = P_i^{(0)} + \delta P_i(t) - \sum_j b_{ij}\sin(\theta_i - \theta_j), \tag{D1}$$

with $i = 1, \ldots, n$, for arbitrary coupling graph.

#### 1. Cycle networks

For cycle networks with nearest-neighbor coupling and identical natural frequencies, the distance between the stable equilibrium $\boldsymbol{\theta}^{(0)} = (0, \ldots, 0)$, and the 1-saddle $\boldsymbol{\varphi}$, can be computed analytically as [21]

$$\Delta^2 = \left\| \boldsymbol{\theta}^{(0)} - \boldsymbol{\varphi} \right\|_2^2 = \frac{n(n^2 - 1)}{12(n - 2)^2}\pi^2. \tag{D2}$$

#### 2. General networks

For general networks, the anisotropy of the basins of attraction renders the 1-saddles complicated to identify analytically. We propose a numerical method to locate 1-saddles, which is based on two results of DeVille [12]:

(1) Escapes from basins of attraction almost always occur in a neighborhood of a 1-saddle of the potential

$$\mathcal{V}(\boldsymbol{\theta}) = \sum_{i=1}^{n} P_i^{(0)}\theta_i - \sum_{i<j} b_{ij}[1 - \cos(\theta_i - \theta_j)]. \tag{D3}$$
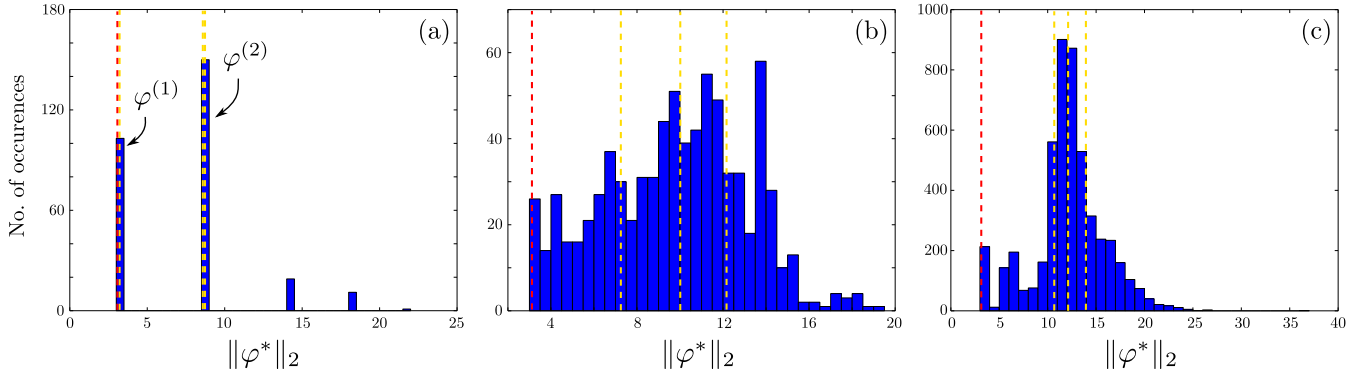
FIG. 9. Histograms of the 2-norm distance from the fixed point of the set of 1-saddles found numerically for the cycle with third-neighbor (a), the U.K. network (b), and the small-world network (c). We found (a) 284 1-saddles for the cycle with third neighbor, with smallest 2-norm $n_{\min} \approx 3.12$, and quartiles of the 2-norms $(Q_1, Q_2, Q_3) \approx (3.12, 8.61, 8.61)$; (b) 788 1-saddles for the U.K. network, with smallest 2-norm $n_{\min} \approx 3.13$, and quartiles of the 2-norms $(Q_1, Q_2, Q_3) \approx (7.24, 10.02, 12.17)$; and (c) 4956 1-saddles for the small-world network, with smallest 2-norm $n_{\min} \approx 3.13$, and quartiles of the 2-norms $(Q_1, Q_2, Q_3) \approx (10.74, 12.13, 13.95)$. The yellow dashed lines indicate the three quartiles $Q_1$, $Q_2$, and $Q_3$, and the red dashed lines indicate the norm of the closest 1-saddle.

(2) Transitions from a basin to another occur on a short time interval compared to the time the system remains in a basin of attraction.

We numerically integrate Eq. (D1), where $\delta P_i$ is a noise with small variance, and keep track of the angles in order to identify iterations where the system is close to a 1-saddle. As observed in Ref. [12], when the system is driven (by the noise) to another basin of attraction, its trajectory goes close to a 1-saddle, and this can be seen in the time evolution of the angles as a fast jump of a set of angles of amplitude $2\pi$ (see Fig. 8). The state $\boldsymbol{\varphi}^{(0)}$ of the system in the middle of this jump will be a candidate for a 1-saddle. This state is probably not exactly a 1-saddle, but according to Ref. [12], it should be close to one. We then solve the steady-state equations

$$P_i^{(0)} = \sum_j b_{ij} \sin(\theta_i - \theta_j), \quad i = 1, \ldots, n, \quad \text{(D4)}$$

using a Newton-Raphson method with initial conditions $\boldsymbol{\varphi}^{(0)}$. This gives an equilibrium $\boldsymbol{\varphi}^*$ of Eq. (D1), which we expect to be close to $\boldsymbol{\theta}^{(0)}$. Computing the eigenvalues of the Jacobian of Eq. (D1), the equilibrium $\boldsymbol{\varphi}^*$ is a $p$-saddle if and only if it

has $p$ positive eigenvalues. Note that one eigenvalue is always zero due to invariance of Eqs. (D1) and (D3) under a constant shift of all angles.

Running this simulation for a long enough time, we identified the following:

(1) 284 1-saddles for the cycle with nearest and third neighbor. The distribution of their distance to the stable equilibrium $\boldsymbol{\theta}^{(0)}$ is given in Fig. 9(a). Looking more into details, we observe that each value in Fig. 9(a) corresponds to a unique 1-saddle, up to an index shift or the angles' sign reversal. The 1-saddles with the two smallest norm, $\boldsymbol{\varphi}^{(1)}$ and $\boldsymbol{\varphi}^{(2)}$, are represented in Fig. 10. The first one [Fig. 10(a)] has the smallest 2-norm, but its configuration with $n - 1$ equal angles and one angle $\pi$ apart from all others is, in our opinion, unlikely to occur. As we consider noisy perturbation at all nodes, a configuration with a single large angle excursion and
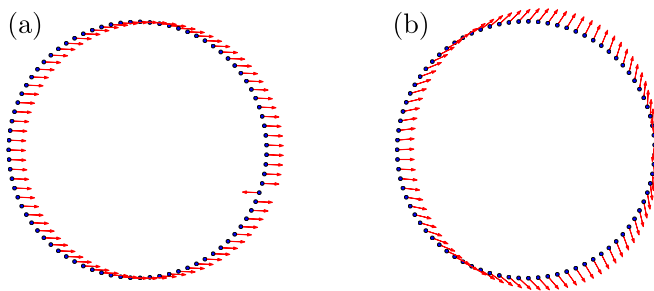


FIG. 10. The two 1-saddles, $\boldsymbol{\varphi}^{(1)}$ and $\boldsymbol{\varphi}^{(2)}$, with smallest 2-norm, for the cycle network, with nearest and third neighbors. (a) $\boldsymbol{\varphi}^{(1)}$: all angles are equal, except one which is $\pi$ apart from all others. The 2-norm of this 1-saddle is $\sim 3.12$. (b) $\boldsymbol{\varphi}^{(2)}$: all angles are slightly displaced compared to their neighbors. The 2-norm of this 1-saddle is $\sim 8.61$. This configuration is, in our opinion, more likely to occur under noisy perturbations applied to all nodes.
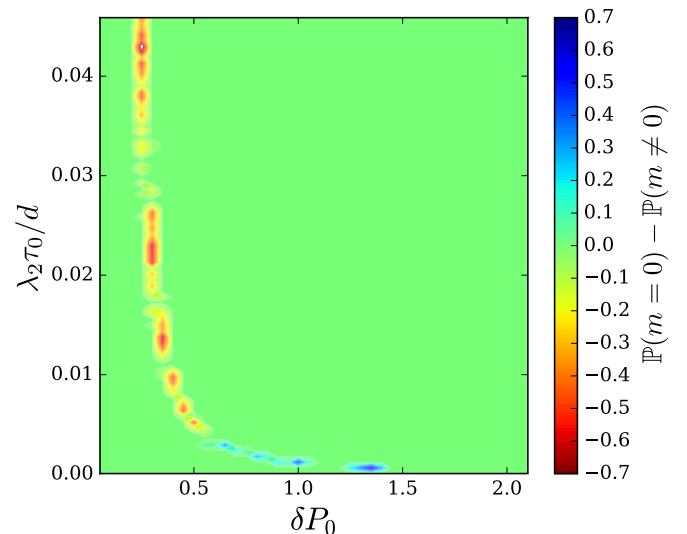


FIG. 11. Color plot of the difference of fraction of trajectories that stay in the initial basin of attraction with finite inertia compared to $m = 0$ for a cycle network of $n = 83$ nodes. Timescales are $\frac{m}{d} / \frac{d}{\lambda_2} = 10/175$.

no excursion for all other nodes seems less likely than a configuration where all angles are slightly displaced from their neighbors. In the main text, we performed our study using $\boldsymbol{\varphi}^{(2)}$ as 1-saddle for the cycle with nearest and third neighbor.

(2) 788 1-saddles for the U.K. network, whose distribution of the distances to the stable equilibrium is given in Fig. 9(b). Distances cover a large range of value, due to the anisotropy of the basin of attraction.

(3) 4956 1-saddles for the small-world network. The distribution of the distances to $\boldsymbol{\theta}^{(0)}$ is given in Fig. 9(c). Most of the 1-saddles are at a similar distance.

## APPENDIX E: LINEARIZATION BREAKDOWN

In the main text, we show that, according to our theory, inertia always destabilizes the system compared to the inertialess case. However, for the cycle network, we found that for small $\tau_0$ and large $\delta P_0$, inertia stabilizes the system, as illustrated in Fig. 11. The blue area where inertia stabilized the system is not predicted by our theory [Eq. (8)]. This can be explained by the breakdown of the linear approximation. Indeed, the blue region in Fig. 11 starts for the value of the order of the coupling $\delta P_0 \cong b_0 \equiv 1$.

[1] E. Ott, *Chaos in Dynamical Systems*, 2nd ed. (Cambridge University Press, Cambridge, 2002).

[2] N. G. Van Kampen, Phys. Rep. **24**, 171 (1976).

[3] J. Machowski, J. W. Bialek, and J. R. Bumby, *Power System Dynamics*, 2nd ed. (Wiley, Chichester, UK, 2008).

[4] S. Auer, F. Hellmann, M. Krause, and J. Kurths, Chaos **27**, 127003 (2017).

[5] B. Schäfer, M. Matthiae, X. Zhang, M. Rohden, M. Timme, and D. Witthaut, Phys. Rev. E **95**, 060203(R) (2017).

[6] C. E. Gough, M. S. Colclough, E. M. Forgan, R. G. Jordan, M. Keene, C. M. Muirhead, A. I. M. Rae, N. Thomas, J. S. Abell, and S. Sutton, Nature (London) **326**, 855 (1987).

[7] E. Il'ichev and A. N. Omelyanchouk, Low Temp. Phys. **34**, 413 (2008).

[8] H. A. Braun, H. Wissing, K. Schäfer, and M. C. Hirsch, Nature (London) **367**, 270 (1994).

[9] Y. Liu, C. Rui, and J. Duan, arXiv:1811.10960.

[10] H. Kramers, Physica **7**, 284 (1940).

[11] M. I. Dykman, Phys. Rev. A **42**, 2020 (1990).

[12] L. DeVille, Nonlinearity **25**, 1473 (2012).

[13] J. Hindes and I. B. Schwartz, Phys. Rev. Lett. **117**, 028302 (2016).

[14] J. Hindes and I. B. Schwartz, Chaos **28**, 071106 (2018).

[15] D. Lee, I.-L. Aolaritei, T. L. Vu, and K. Turitsyn, IEEE Trans. Cont. Netw. Sys., 1 (2019).

[16] B. Bamieh, M. R. Jovanovic, P. Mitra, and S. Patterson, IEEE Trans. Autom. Control **57**, 2235 (2012).

[17] M. Tyloo, T. Coletta, and P. Jacquod, Phys. Rev. Lett. **120**, 084101 (2018).

[18] H. Haehne, K. Schmietendorf, S. Tamrakar, J. Peinke, and S. Kettemann, Phys. Rev. E **99**, 050301(R) (2019).

[19] D. A. Wiley, S. H. Strogatz, and M. Girvan, Chaos **16**, 015103 (2006).

[20] P. J. Menck, J. Heitzig, N. Marwan, and J. Kurths, Nat. Phys. **9**, 89 (2013).

[21] R. Delabays, M. Tyloo, and P. Jacquod, Chaos **27**, 103109 (2017).

[22] D. Piovani, J. Grujić, and H. J. Jensen, J. Phys. A **49**, 295102 (2016).

[23] Y. Kuramoto, in *International Symposium on Mathematical Problems in Theoretical Physics*, edited by H. Araki, Lecture Notes in Physics Vol. 39 (Springer, Berlin, 1975), pp. 420–422.

[24] M. Tyloo, L. Pagnier, and P. Jacquod, arXiv:1810.09694.

[25] D. J. Klein and M. Randić, J. Math. Chem. **12**, 81 (1993).

[26] D. J. Watts and S. H. Strogatz, Nature (London) **393**, 440 (1998).

[27] F. Dörfler, M. Chertkov, and F. Bullo, Proc. Natl. Acad. Sci. USA **110**, 2005 (2013).

[28] R. Delabays, T. Coletta, and P. Jacquod, J. Math. Phys. **58**, 032703 (2017).

[29] D. Manik, M. Timme, and D. Witthaut, Chaos **27**, 083123 (2017).

[30] R. Delabays, T. Coletta, and P. Jacquod, J. Math. Phys. **57**, 032701 (2016).

[31] T. Giamarchi, *Quantum Physics in One Dimension* (Oxford University Press, Oxford, 2004).